Structure and mechanism of ADP-ribose-1″-monophosphatase (Appr-1″-pase), a ubiquitous cellular processing enzyme

DESIGAN KUMARAN, SUBRAMANIAM ESWARAMOORTHY, F. WILLIAM STUDIER, AND SUBRAMANYAM SWAMINATHAN

Biology Department, Brookhaven National Laboratory, Upton, New York 11973, USA

(RECEIVED September 18, 2004; FINAL REVISION November 25, 2004; ACCEPTED November 29, 2004)

Abstract

Appr-1″-pase, an important and ubiquitous cellular processing enzyme involved in the tRNA splicing pathway, catalyzes the conversion of ADP-ribose-1″monophosphate (Appr-1″-p) to ADP-ribose. The structures of the native enzyme from the yeast and its complex with ADP-ribose were determined to 1.9 Å and 2.05 Å, respectively. Analysis of the three-dimensional structure of this protein, selected as a target in a structural genomics project, reveals its putative function and provides clues to the catalytic mechanism. The structure of the 284-amino acid protein shows a two-domain architecture consisting of a three-layer αβα sandwich N-terminal domain connected to a small C-terminal helical domain. The structure of Appr-1″-pase in complex with the product, ADP-ribose, reveals an active-site water molecule poised for nucleophilic attack on the terminal phosphate group. Loop-region residues Asn 80, Asp 90, and His 145 may form a catalytic triad.

Keywords: ADP-ribose-1″-monophosphate; tRNA splicing pathway; structural genomics; X-ray structure

ADP-ribose 1″,2″-cyclic phosphate (Appr>p) and ADP-ribose-1″ monophosphate (Appr-1″-p) are intermediates in a recently described metabolic pathway involved in pre-tRNA splicing (Culver et al. 1994). Pre-tRNA splicing is initiated by endonucleolytic cleavages that remove the intron and form two tRNA half-molecules. In yeast and plants, the two tRNA exons are ligated in a 3′ to 5′ phosphodiester bond but the resulting molecule retains an adjacent 2′ phosphomonoester group at the splice junction, a pathway that is also conserved in vertebrates except that no 2′ phosphorylated tRNAs formed (Phizicky and Greer 1993). The 2′ phosphate present in the spliced tRNA is removed by a specific phosphotransferase, previously identified in yeast and vertebrates, which transfers the 2′ phosphate to an NAD acceptor molecule, to produce ADP-ribose 1″,2″-cyclic phosphate (Appr>p). However, Appr>p is not the final product of this complex series of reactions. Appr>p is converted into ADP-ribose 1″-phosphate (Appr-1″-p) by the action of a cyclic phosphodiesterase (CPDase) identified in yeast and wheat (Culver et al. 1994; Martzen et al. 1999; Hofmann et al. 2000). It has been suggested that Appr>p, or its hydrolysis product, may perform some as yet unspecified regulatory function(s) in the cell. There is probably a second step where Appr-1″-p is hydrolyzed to ADP-ribose (Martzen et al. 1999). Furthermore, ADP-ribose pyrophosphatase (ADPRase), a nudix enzyme, catalyses the hydrolysis of ADP-ribose to ribose-5-phosphate and AMP, compounds that can be recycled as part of nucleotide metabolism (Gabelli et al. 2001).

Reprint requests to: Subramanyam Swaminathan, Biology Department, Brookhaven National Laboratory, Upton, NY 11973, USA; e-mail: swami@bnl.gov; fax: (631) 344-3407.

Article and publication are at http://www.proteinscience.org/cgi/doi/10.1110/ps.041132005.

$$\text{tRNA splicing} \longrightarrow \text{ADP-ribose } 1'',2''\text{-cyclic phosphate}$$
$$(\text{Appr>p}) \xrightarrow{\text{CPDase}} \text{ADP-ribose-}1'' \text{ phosphate} \xrightarrow{\text{Appr-}1''\text{-pase}}$$
$$\text{ADP-ribose} \xrightarrow{\text{ADPRase}} \text{AMP} + \text{ribose-5-phosphate}$$

Biochemical characterization, structure, and enzymatic mechanisms of CPDase (Genschik et al. 1997; Hofmann et al. 2001) and ADPRase (Gabelli et al. 2001, 2002) have been studied extensively. However, the postulated conversion of ADP-ribose-1″ phosphate to ADP-ribose has not previously been demonstrated or studied.

In this article we identify the yeast protein responsible for Appr-1″-p processing, report the cloning, expression, purification, crystallization, and structure determination of this enzyme and its complex with ADP-ribose, and propose an enzymatic mechanism. A 32.1-kDa hypothetical yeast protein (SwissProt YMX7_YEAST) in the ADH3-RCA1 region was selected in a structural genomics project that is surveying structure–function relationships of proteins identified by genome sequencing (http://www.nysgrc.org). A family of proteins containing only this domain has members from bacteria (SwissProt P75918), archaebacteria (O59182), and eukaryotes (Q17432), suggesting that it is involved in an important and ubiquitous cellular process. In addition, this domain is found in a number of multidomain proteins, including the C terminus of the macro-H2A histone protein (Q02874) and in nonstructural proteins of several types of ssRNA viruses, such as NSP2 from alphaviruses (P03317). The SMART database (Schultz et al. 1998; Letunic et al. 2002) identifies this domain as an Appr-1″-p processing enzyme, based on the extended family detection by reciprocal PSI-BLAST searches and the identification of the activity of one of the members by biochemical genomic approach (Pehrson and Fuji 1998; Martzen et al. 1999; Bateman et al. 2002). Approximately 300 proteins have so far been identified with this motif, called A1pp domain, and they have no significant sequence homology with proteins of known structure.

Results and Discussion

Structure determination

The yeast protein YMX7_YEAST was cloned and expressed as described in the Materials and Methods section. The crystal structure has been determined to a 2.6 Å resolution by the multiple wavelength anomalous dispersion method (MAD) using the SelenoMet protein. The heavy atom phase refinement was carried out with SHARP (De La Fortelle and Bricogne 1997), and the phases were further improved by density modification. The model building and initial refinements were completed with this improved set of phases. Further refinements were carried out with 1.9 Å resolution data collected from a second SelenoMet crystal. The final model consists of 245 residues, 128 water molecules, and one xylitol molecule, which was used as additive during crystallization. Thirty-nine residues are missing in the loop regions. The crystallographic *R*-factor is 0.20 (*R*-free = 0.23) for 18,988 reflections in the resolution range of 50–1.9 Å. The final model has good stereochemistry with 92% of the residues in the most favored region of the Ramachandran plot.

Description of the structure

In the crystal structure, Appr-1″-pase exists as a dimer with dimensions of $65 \times 67 \times 50$ Å^3. A monomer consists of two domains, with residues 16–219 forming an α/β domain (Domain 1 or N-terminal) with a unique topology and residues 220–279 (Domain 2 or C-terminal) forming a helical bundle (Fig. 1A). The core of the α/β domain is a six-stranded β-pleated sheet. The order of the β-strands in the β-sheet is β2, β1, β6, β3, β5, and β4. Except for strand β4, the others are parallel. The β-pleated sheet is flanked by three prominent helices, α2, α3, and α4, on one side, and α1, α5, and α6 on the other (Fig. 1B). The region between the α-helices and the β-sheet is hydrophobic. The interface between the two domains is also highly hydrophobic. Domain 2 consists of two α-helices (α7 and α8) and four 3_{10} helices. A helical axis of the α8 is orthogonal to the axes of the other α and 3_{10} helices. Helix α7 and the terminal 3_{10} helix have strong interactions with Domain 1.

Fold identification

A Dali (Holm and Sander 1996) and TOPS (Gilbert et al. 1999) database search with Appr-1″-pase as a model gave no structure with a *z*-score greater than 6.7 or a topology rank less than 28, indicating that the fold may be unique. The closest structure (*z*-score = 6.7) identified by Dali is leucine aminopeptidase (Burley et al. 1990), which, however, has an α/β fold for both domains. Also, the number and order of strands are different from Appr-1″-pase. While leucine aminopeptidase has two zinc ions in the active site, Appr-1″-pase has no metal atom, at least in the crystal structure. TOPS gave the closest topology (Topology rank = 28) with flavodoxin reductase (Ingelman et al. 1997). Again, this is a two domain-structure with an α/β fold. Even though it is Rossmann or an ATP-binding protein fold, its topology and domain organization are different from the other known nucleotide-binding protein structures.

Dimeric association

Appr-1″-pase dimer is formed via a crystallographic twofold axis with approximately a 2906 Å^2 buried surface area. The

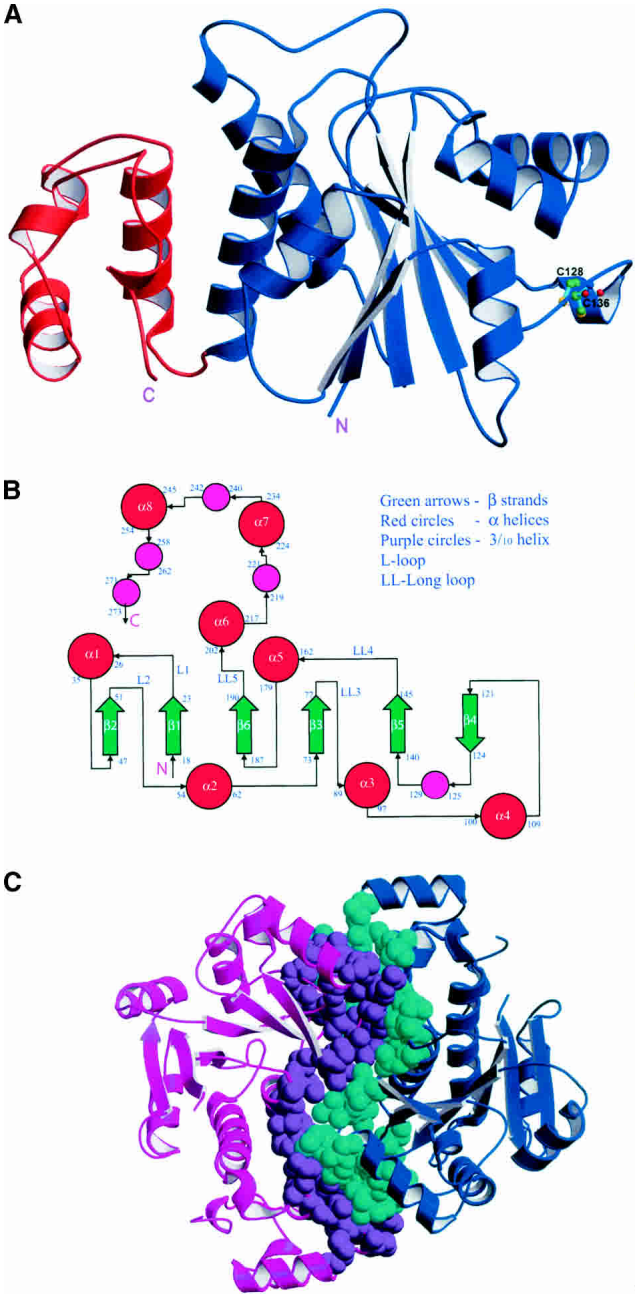

Figure 1. (*A*) Ribbons representation of a monomer of Appr-1″-pase. Domains 1 and 2 are shown in blue and red, respectively. Cys residues involved in disulfide bond are shown as a ball-and-stick model. This figure was prepared with Molscript and Raster3D (Kraulis 1991; Merritt 1994). (*B*) Topology diagram for ADP-ribose-1″-monophosphatase. (*C*) Dimeric association of Appr-1″-pase. The two monomers are shown in purple and blue. Residues involved in stacking interaction, salt bridges, and hydrogen bonds at the interface are shown as a sphere model.

helical layer of Domain 1 of monomer A has strong interactions with the helical layer of Domain 2 of monomer B and vice versa (Fig. 1C). The dimeric molecule is wedge shaped. The loops formed at the C-terminal ends of β3 (80–83), α4 (112–118), and β5 (150–161) of domain 1 of monomer A have strong interactions with α7 and the 3_{10} helix (224–243) of Domain 2 of monomer B. While the C-terminal ends of β3, α4, and β7 of the two protomers are close together, the N-terminal ends are farthest apart, forming a wedge. These regions are filled with water molecules making strong hydrogen bonds with protein residues. There is one hydrophobic region formed by residues Phe 171, Trp 175, Leu 231, and Leu 235 of monomer A and Tyr 114 and Val 150 of monomer B in the dimeric interface. This hydrophobic core is followed by stacking interactions in the order one above the other, Arg 107, Tyr 84, and Phe 242 of monomer A and Phe 239 of monomer B. Apart from these, one salt bridge is formed between Asp 225 of monomer A with Arg 107 of monomer B in addition to hydrogen bonds. OE1 and NE2 of Gln 160 of monomer A make strong hydrogen bonds with NE2 and OE1 of Gln 160 of monomer B. Four water molecules were located in the interface.

Binding site

In the native structure, a deep pocket has been identified in a crevice formed by the C-terminal ends of strands β3 and β5, and is typical of the binding site in the Rossmann fold. This pocket is lined with residues Pro 78, Gly 79, Asn 80, Gly 86, Gly 87, Gly 88, Phe 89, Asp 90, Thr 148, Val 149, Pro 152, Ala 154, Pro 191, Gly 192, Leu 193, Cys 194, Thr 195, Gly 196, Tyr 197, and Ala 198. These residues are mainly located in the loop regions LL3, LL4, and LL5. One xylitol molecule is bound in this cleft. It makes strong hydrogen bonds with Asp 23 OD1, Phe 89 N, and through water molecules with N and O of Cys 194 and Gly 52, respectively (Fig. 2). The substrate binding may involve this region.

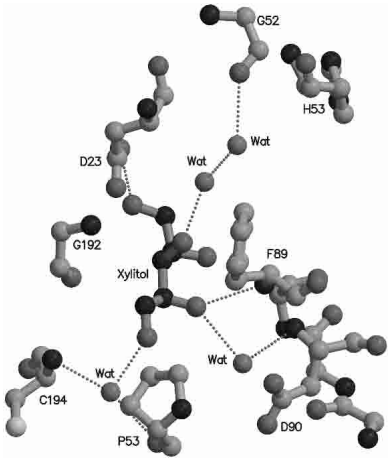

Figure 2. Ball-and-stick representation of xylitol and interacting protein residues with water molecules. The dashed lines indicate hydrogen bonding.

Appr-1″-pase:ADP-ribose complex

ADP-ribose binding

Appr-1″-pase coordinates were used as a starting model with the data collected from the Appr-1″-pase:ADP-ribose complex crystal. A model of ADP-ribose has been fitted in the difference Fourier map calculated after the rigid-body refinement followed by simulated annealing with CNS (Fig. 3A). In addition to ADP-ribose, two sulfate ions, one sodium ion and one ethylene glycol molecule, were identified, which were all present in the crystallization condition. One of the sulfate ions is bound at the dimeric interface and makes hydrogen bonds with Asn 176 and His 180. Another sulfate ion is bound at the surface of the N-terminal domain and forms hydrogen bonds with His 53 and Asn 95 of a symmetry-related molecule.

ADP-ribose binds in the cleft identified as a xylitol-binding site in the native structure and displaces a few water molecules. It is tightly bound in the crevice at the tip of the β-sheet, mainly on strands β1, β3, β5, and β6, and is

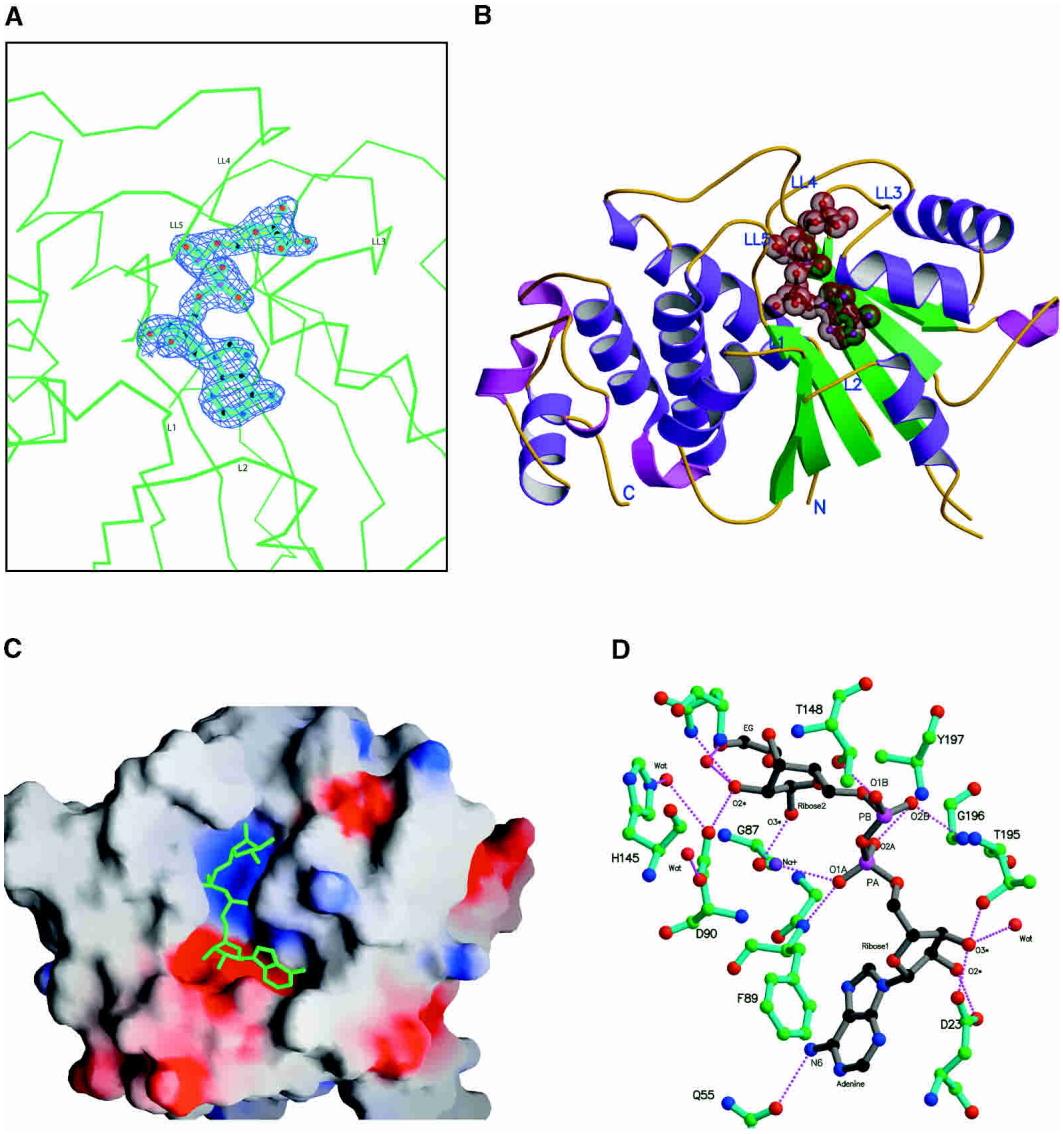

Figure 3. (*A*) Fo–Fc map contoured at the 3σ level with the refined ADP ribose molecule superposed and the C-α trace in the nearby region shown as a line drawing. (*B*) Location of ADP-ribose binding with Appr-1″-pase. Bound ADP-ribose is shown in ball and stick embedded in a space-filling model. ADP-ribose binds at the top of the β sheet and is surrounded by loops (L1, L2, LL3, LL4, and LL5). (*C*) Electrostatic potential surface representation (Nicholls et al. 1991) of the active site cavity. ADP-ribose is shown in a stick model in green color. (*D*) Closeup view of the interactions between Appr-1″-pase and ADP-ribose in a ball-and-stick representation. Bonds of protein residues and ADP-ribose are shown in cyan and gray, respectively. Carbon, oxygen, nitrogen, and phosphorus atoms are shown in green, red, blue, and purple, respectively. The purple dashed lines indicate the hydrogen bonding.

wrapped around by the small loops L1 and L2, and large loops LL3, LL4, and LL5 (Fig. 3B). The electrostatic potential surface of the Appr-1″-pase molecule reveals an open and solvent accessible binding site (expect Tyr 197) in LL5 with negatively and positively charged floors (Fig. 3C). The only significant difference between the structures in the presence and absence of ADP-ribose is observed in the conformation of loop (LL3) residues Leu 85, Gly 86, Gly 87, Gly 88, and Phe 89 and the loop (LL5) formed by residues Gly196, Tyr 197, and Ala 198. These two loops have no clear electron density in the native structure but they are well ordered in the structure of the ADP-ribose complex probably due to stabilizing interactions provided by ADP-ribose.

Bound ADP-ribose is a C-shaped structure, and the adenine ring makes an angle of approximately 45° with the terminal ribose ring in the Appr-1″-pase structure (Fig. 3B), which is different from ADP-ribose bound to the Nudix hydrolase ADPRase, where it resembles a horse shoe. In the Appr-1″-pase complex with ADP-ribose, the adenosine group of the ADP-ribose binds to the enzyme in the *anti* conformation, which is evident from the glycosylic bond torsion angle (–94°). The adenine base is sitting on the hydrophobic pocket formed by residues Leu 54, Phe 89, and Ala 92. The N6 atom of the adenine ring makes one hydrogen bond with Gln 55, and the N1 atom is free, which is in contrast to other ATP-binding proteins, where both N1 and N6 are involved in hydrogen bonding. The O2* and O3* of the ribose (ribose1) make strong hydrogen bonds with carboxylate atoms of Asp 23 in addition to a water molecule and Thr 195 (Fig. 3D). α and β phosphate groups of the ADPR are buried in the cleft formed by the Appr-1″-pase with respect to the adenine and terminal ribose ring. The charge of the α-phosphate is neutralized by the sodium ions. The positively charged region seen in Figure 3C is probably due to this and the main-chain amide groups. Both α and β

Table 1. *Crystal data, data collection, phasing, and refinement statistics for Appr-1″-pase and Appr-1″-pase:ADP-ribose complex*

Cell dimensions	$a = 107.69$, $b = 38.15$, $c = 64.74$ Å and $\beta = 112.21°$			
Space group C2				
	Crystal I		Crystal II	
	Edge	Peak		P089+ADPR
Wavelength (Å)	0.9786	0.9785	0.9785	1.000
Resolution range	50.0–2.6	50.0–2.2	50.0–1.9	50.0–2.05
(outer shell)	(2.69–2.6)	(2.28–2.2)	(1.97–1.9)	(2.12–2.05)
Unique reflections	7,784	12,591	18,988	14,181
Completeness (%)				
Overall (outer shell)	99.6 (95.5)	99.4 (94.3)	97.8 (84.4)	95.3 (69.0)
R_{merge}[a] (outer shell)	0.065 (0.20)	0.07 (0.31)	0.117 (0.27)	0.028 (0.16)
Phasing power[b] (ano)	2.2	2.8		
FOM:[c] MAD (centric/acentric)		0.38/0.63		
After solvent flattened		0.93		
Refinement statistics:				
R-factor[d]/free_R			0.20/0.23	0.20/0.23
Resolution range (Å)			50.0–1.9	50.0–2.05
Number of atoms				
Proteins			1978	1978
Waters			112	88
Ligands				36
Ions				12
RMS deviation from ideality				
Bonds (Å)			0.01	0.01
Angles (°)			1.21	1.52
Average B-factors (Å^2)				
Main chain			31	33
Side chain			35	36
Solvent			37	36
Ligand (ADPR)				27
Ions				34

[a] $R_{merge} = \sum_j(|I_h - \langle I\rangle_h|)/\sum I_h$ where $\langle I_h\rangle$ is the average intensity over symmetry equivalents.
[b] Phasing power and [c]FOM (figure of merit) are as defined in SHARP (De La Fortelle and Bricogne 1997).
[d] R-factor $= \sum|F_{obs} - F_{calc}|/\sum|F_{obs}|$.

phosphates make strong hydrogen bonds with main-chain atoms. Interestingly, there is no Arg or Lys in this region to have interactions with α and β phosphate groups, which is usually observed in proteins containing a typical nucleotide-binding domain. In this structure the closest lysine (Lys 91) is 9.8 Å from the terminal ribose oxygen, O2*.

The terminal ribose ring is buried in the cleft closer to the opening and pointing toward the solvent region. An ethylene glycol molecule binds to this terminal ribose ring through a water molecule (Fig. 3D). The O2* atom of the terminal ribose makes a strong hydrogen bond network with residues Asp 90, His 145, Asn 80, and a structural water molecule of Appr-1″-pase. The structure of the complex between ADP-ribose and Appr-1″-pase reveals unambiguously the location and extent of binding.

A probable scheme for catalytic mechanism

Based on the ADP-ribose binding to Appr-1″-pase, we have modeled the Appr-1″-p in the active site. We positioned the ADP-ribose1″-monophosphate in the place of ADP-ribose with slight changes in the protein residues Tyr 197 and Asn 83 and terminal ribose sugar of the ADP-ribose to relieve short contacts. The molecule fits well in the cavity and the terminal phosphate group interacts with the protein residues. Interestingly, there is one structural water (w2) molecule, which is about 3.7 Å from the phosphorus atom of the terminal phosphate group, making a hydrogen-bond network with Asp 90 and His 145 through another structural water (w5) (Fig. 4A). Terminal phosphate oxygen atom O1 forms a hydrogen bond with Gly 86 N, and Gly 86 O makes a hydrogen bond with Lys 91 NZ. Phosphate oxygen O2 forms a hydrogen bond with one water molecule (w88) and O3 with Asn 80. Based on this binding environment and hydrogen-bond network with water molecules, we propose the following scheme for catalytic mechanism.

Asp 90 in its unprotonated form is probably activated by His 145 through water w5 and removes a proton from the water. The resulting hydroxide ion attacks the terminal phosphate as nucleophile, which is at the proper distance (3.7 Å), although the water–phosphorus–oxygen angle is not ideal (Fig. 4B). In this scenario, Asp 90 is the catalytic base. This complex most likely passes through trigonal-bipyramidal geometry similar to RNAse (Wlodawer and Sjolin 1983) and CPDase (Hofmann et al. 2000). In the second step, Asp 90 transfers its proton to ribosyl oxygen, to yield ADP-ribose. Asn 80, Gly 86, Lys 91, and water 88 probably act as stabilizing groups by interacting with the phosphate oxygens. Based on this analysis, we favor Asp 90 as the initiating residue of catalysis with the help of His 145, and propose that Asp 90, His 145, and Asn 80 form a catalytic triad.

Materials and methods

Enzyme preparation and crystallization

The coding sequence for P089 was amplified from yeast DNA and cloned in the NdeI and BamHI sites in the pET-13a vector (Gerchman et al. 1994). DNA sequencing verified that the coding sequence was correct. P089 protein was expressed in B834(DE3) (Studier and Moffatt 1986) carrying the RIL plasmid to supply rare tRNAs (Stratagene). A culture of the expression strain grown at 37°C in 400 mL of ZYP-5052 auto-inducing medium in a 1.8-liter baffled Fernbach flask (Bellco) yielded 12.3 mg of purified protein, and a second 400-mL culture grown in PASM-5052 auto-inducing medium yielded 4 mg of purified SeMet-labeled protein. (Recipes and protocols for autoinduction, to be described elsewhere, are available by e-mail request to studier@bnl.gov.) The P089 protein appeared to be only partially soluble at both 20°C and 37°C.

Cells were lysed in Bugbuster + Benzonase (Novagen). The P089 protein was purified by chromatography on a 2.5 cm × 17 cm Fractogel EMD SO3 650(M) column at room temperature in a gradient of 0–1 M NaCl in 10 mM Tris-Cl (pH 8.0), followed by gel filtration at 4°C on a 2.5 cm × 60 cm Superdex 75 column in 300 mM NaCl, 10 mM Tris-Cl (pH 8.0) (natural protein) or 125 mM ammonium sulfate, 10 mM Tris-Cl (pH 8.0) (SeMet protein). The purified protein appeared to elute from the gel-filtration column as a dimer. Purification was followed by gel electrophoresis in the presence of sodium dodecyl sulfate. The P089 protein band was identified by its intensity and position relative to the pattern of total proteins of induced cells, staining the gel with Coomassie blue. The natural protein was concentrated to approximately 6 mg/mL and stored in 250 mM NaCl, 10 mM Tris-Cl (pH 8.0). The SeMet protein was concentrated to approximately 6 mg/mL and stored in 125 mM ammonium sulfate, 10 mM Tris-Cl (pH 8.0).

Initial crystallization conditions were obtained with the use of Hampton Research Crystal Screens but restricting the trials to pH values close to the pI (5.5) of the protein. Two microliters of protein at a concentration of 6.0 mg mL^{-1} and 2 μL of the precipitant were placed in a microbridge, which was in turn placed inside Linbro plate wells containing appropriate precipitants. The wells were sealed with clear tape and left at room temperature. Initial trials gave microcrystals in a wide range of conditions with various PEGs and pH ranges (5.0–7.0). Good-quality native crystals were obtained in 18% PEG 6K, 100 mM citric acid (pH 5.0), 3% xylitol, and 200 mM LiCl. Long rectangular bar-like crystals with dimension $0.2 \times 0.15 \times 0.30$ mm^3 were obtained within a week. These crystals diffracted to better than 2.5 Å resolution. Crystals were flash frozen by adding 20% glycerol to the mother liquor before the crystal was mounted on a Hampton loop.

To determine the structure, selenomethionine-labeled protein was used. Crystals of the SeMet P089 protein were grown in conditions similar to those for the native sample by the vapor diffusion in sitting drops at room temperature. Equal volumes of protein (6 mg/mL) and a solution containing 20% PEG 6K in 75 mM citric acid (pH 5.0), with 3% xylitol and 500 mM NH_4Cl were mixed and equilibrated against a 800-μL reservoir containing the same precipitant solution.

Data collection and structure determination

MAD data extending to 2.2 Å were collected near the selenium absorption edge from a single crystal at liquid nitrogen temperature using the Brandeis 4 detector at beamline X12C of the National Synchrotron Light Source (NSLS).

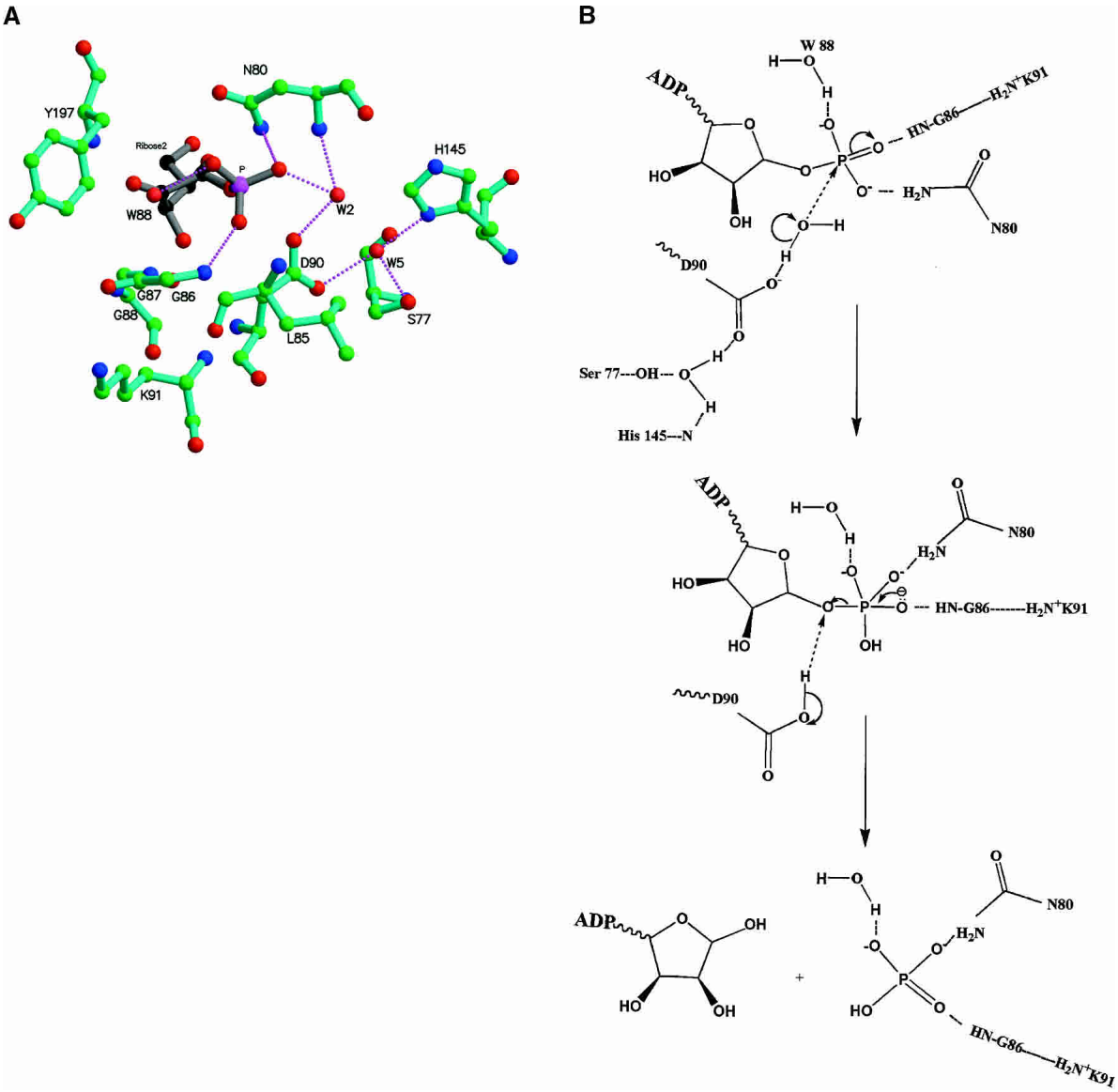

Figure 4. (*A*) Closeup view of the interactions between Appr-1″-pase and ADP-ribose-1″ phosphate in a ball-and-stick representation. For clarity, only terminal ribose ring with the modeled phosphate group is shown. Bonds of protein residues and ADP-ribose are shown in cyan and gray, respectively. Carbon, oxygen, nitrogen, and phosphorus atoms are shown in green, red, blue, and purple, respectively. The purple dashed lines indicate the hydrogen bonding. (*B*) Proposed scheme for a catalytic mechanism (see text for details).

Data were reduced with HKL2000 (Otwinowski and Minor 1997) and the data collection statistics are given in Table 1. Crystals belong to the monoclinic space group C2 with cell dimensions, $a = 107.69, b = 38.15, c = 64.74$ Å, and $\beta = 112.21°$ (Table 1). Assuming one molecule of 32,067 Da per asymmetric unit, the Matthews coefficient (Matthews 1968) is 1.89 $Å^3$/Da, corresponding to an estimated solvent content of 35% by volume of the unit cell. This crystal undergoes radiation damage. At the end of the high-energy remote data, the crystal diffracted to only 2.7 Å.

Seven out of nine selenium positions were obtained from the Patterson and difference Fourier maps using the program SOLVE (Terwilliger and Berendzen 1997), and phase refinement was carried out with SHARP (De La Fortelle and Bricogne 1997). Since the crystal suffers radiation damage, only peak and edge data up to 2.6 Å were used for phasing. Single-wavelength higher resolution data extending to 1.9 Å were collected with a better quality selenomethionine crystal at ×25 beamline, NSLS (Table 1). The resulting 2.6 Å phases were further extended to 1.9 Å in DM (Cowtan 1994). The resulting electron density map was of excellent quality and revealed almost all of the secondary structure. ARP/wARP (Perrakis et al. 1999) built 70% of the chain and the rest was traced manually using the "baton" option in "O" (Jones et al. 1991). Twelve percent of the residues in the loop regions are missing from the electron density. Model was refined with CNS (Brunger et al. 1998) by the slow-cool annealing method, alternating with model building until convergence. The final refinement statistics are given in Table 1. The coordinates have been deposited with the Protein Data Bank (PDB ID 1NJR).

Complex ADP-ribose and Appr-1″-p

Appr-1″-pase was co-crystallized with ADP-ribose by vapor diffusion in sitting drops at room temperature. Equal volumes of protein (6 mg/mL) mixed with ADP-ribose (50 mM) and a solution containing 25% PEG 3350 in 100 mM bis-tris (pH 5.0), with 5% ethylene glycol and 200 mM $LiSO_4$ were mixed and equilibrated against a 800-μL reservoir containing the same precipitant solution. The structure of the complex was determined by rigid-body refinement of the native structure. The composite omit map and the difference Fourier clearly showed the electron density for the ADP-ribose in addition to two sulfate ions, one sodium ion and one ethylene glycol. ADP-ribose was modeled in the density and refined with CNS until convergence. The refinement statistics are shown in the Table 1. Coordinates have been deposited with the Protein Data Bank (PDB ID 1TXZ).

Acknowledgments

Research was supported by the NIHealth (GM62529) under Prime Contract no. DEAC02-98CH10886 with the Brookhaven National Laboratory. We thank H. Kycia and S.E. Gerchman for technical help, and Drs. A. Saxena and M. Becker for providing us data collection facilities at the NSLS.

References

Bateman, A., Birney, E., Cerruti, L., Durbin, R., Etwiller, L., Eddy, S.R., Griffiths-Jones, S., Howe, K.L., Marshall, M., and Sonnhammer, E.L. 2002. The Pfam protein families database. *Nucleic Acid Res.* **30:** 276–280.

Brunger, A.T., Adams, P.D., Clore, G.M., Delano, W.L., Gros, P., Grosse-Kunstleve, R.W., Jiang, J.S., Kuszwewski, J., Nilges, M., Pannu, N.S., et al. 1998. Crystallography & NMR system: A new software suite for macromolecular structure determination. *Acta Crystallogr. D Biol. Crystallogr.* **54:** 905–921.

Burley, S.K., David, P.R., Taylor, A., and Lipscomb, W.N. 1990. Molecular structure of leucine aminopeptidase at 2.7 Å resolution. *Proc. Natl. Acad. Sci.* **87:** 6878–6882.

Cowtan, K. 1994. 'DM': An automated procedure for phase improvement by density modification. *Joint CCP4 and ESF-EACBM newsletter on protein crystallography.* **31:** 34–38.

Culver, G.M., Consaul, S.A., Tycowski, K.T., Filipowicz, W., and Phizicky, E.M. 1994. tRNA splicing in yeast and wheat germ. A cyclic phosphodiesterase implicated in the metabolism of ADP-ribose 1″, 2″-cyclic phosphate. *J. Biol. Chem.* **269:** 24928–24934.

De La Fortelle, E. and Bricogne, G. 1997. Maximum-likelihood heavy atom parameter refinement in the MIR and MAD methods. *Methods Enzymol.* **276:** 472–493.

Gabelli, S.B., Bianchet, M.A., Bessman, M.J., and Amzel, L.M. 2001. The structure of ADP-ribose pyrophosphatase reveals the structural basis for the versatility of the Nudix family. *Nat. Struct. Biol.* **8:** 467–472.

Gabelli, S.B., Bianchet, M.A., Ohnishi, Y., Ichikawa, Y., Bessman, M.J., and Amzel, L.M. 2002. Mechanism of the *Escherichia coli* ADP-ribose pyrophosphatase, a Nudix hydrolase. *Biochemistry* **41:** 9279–9285.

Genschik, P., Hall, J., and Filipowicz, W. 1997. Cloning and characterization of the Arabidopsis cyclic phosphodiesterase which hydrolyzes ADP-ribose 1″,2″-cyclic phosphate and nucleoside 2′,3′-cyclic phosphates. *J. Biol. Chem.* **272:** 13211–13219.

Gerchman, S.E., Graziano, V., and Ramakrishnan, V. 1994. Expression of chicken linker histones in *E. coli*: Sources of problems and methods for overcoming some of the difficulties. *Protein Expr. Purif.* **5:** 242–251.

Gilbert, D., Westhead, D., Nagano, N., and Thornton, J. 1999. Motif-based searching in TOPS protein topology databases. *Bioinformatics* **15:** 317–326.

Hofmann, A., Zdanov, A., Genschik, P., Ruvinov, S., Filipowicz, W., and Wlodawer, A. 2000. Structure and mechanism of activity of the cyclic phosphodiesterase of Appr>p, a product of the tRNA splicing reaction. *EMBO J.* **19:** 6207–6217.

Holm, L. and Sander, C. 1996. Mapping the protein universe. *Science* **273:** 595–603.

Ingelman, M., Bianchi, V., and Eklund, H. 1997. The three-dimensional structure of flavodoxin reductase from *Escherichia coli* at 1.7 Å resolution. *J. Mol. Biol.* **268:** 147–157.

Jones, T.A., Zou, J., Cowtan, S., and Kjeldgaard, M. 1991. Improved methods in building protein models in electron density map and the location of errors in these models. *Acta Crystallogr. A* **47:** 110–119.

Kraulis, P.J. 1991. MOLSCRIPT: A program to produce both detailed and schematic plots of proteins. *J. Appl. Crystallogr.* **24:** 946–950.

Letunic, I., Goodstadt, L., Dickens, N.J., Doerks, T., Schultz, J., Mott, R., Ciccarelli, F., Copley, R.R., Ponting, C.P., and Bork, P. 2002. Recent improvements to the SMART domain-based sequence annotation resource. *Nucleic Acid Res.* **30:** 242–244.

Martzen, M.R., McCraith, S.M., Spinelli, S.L., Torres, F.M., Fields, S., Grayhack, E.J., and Phizicky, E.M. 1999. A biochemical genomics approach for identifying genes by the activity of their products. *Science* **286:** 1153–1155.

Matthews, B.W. 1968. Solvent content of protein cyrstals. *J. Mol. Biol.* **33:** 491–497.

Merritt, E.A. 1994. Raster3D version 2.0. A program for photorealistic molecular graphics. *Acta Crystallogr. D Biol. Crystallogr.* **50:** 869–873.

Nicholls, A., Sharp, K.A., and Honig, B. 1991. Protein folding and association: Insights from the interfacial and thermodynamic properties of hydrocarbons. *Proteins* **11:** 281–296.

Otwinowski, Z. and Minor, W. 1997. Processing of X-ray diffraction data collected in oscillation mode. *Methods Enzymol.* **276:** 307–326.

Pehrson, J.R. and Fuji, R.N. 1998. Evolutionary conservation of histone macroH2A subtypes and domains. *Nucleic Acid Res.* **26:** 2837–2842.

Perrakis, A., Morris, R., and Lamzin, V.S. 1999. Automated protein model building combined with iterative structure refinement. *Nat. Struct. Biol.* **6:** 458–463.

Phizicky, E.M. and Greer, C.L. 1993. Pre-tRNA splicing: Variation on a theme or exception to the rule? *Trends Biochem. Sci.* **18:** 31–34.

Schultz, J., Milpetz, F., Bork, P., and Ponting, C.P. 1998. SMART, a simple modular architecture research tool: Identification of signaling domains. *Proc. Natl. Acad. Sci.* **95:** 5857–5864.

Studier, F.W. and Moffatt, B.A. 1986. Use of bacteriophage T7 RNA polymerase to direct selective high-level expression of cloned genes. *J. Mol. Biol.* **189:** 113–130.

Terwilliger, T.C. and Berendzen, J. 1997. Automated structure solution for MIR and MAD. *Acta Crystallogr. D Biol. Crystallogr.* **55:** 849–861.

Wlodawer, A. and Sjolin, L. 1983. Structure of ribonuclease A: A result of joint neutron and X-ray refinement at 2.0 Å resolutiom. *Biochemistry* **22:** 2720–2728.